InAlGaAs/InAlAs MQWs on Si Substrate

Bei Shi, Qiang Li, Yating Wan, Kar Wei Ng, Xinbo Zou, *Member, IEEE*,
Chak Wah Tang, and Kei May Lau, *Fellow, IEEE*

***Abstract*— We report the growth and characterization of InAlGaAs/InAlAs multiquantum wells (MQWs) emitting at ∼1310-nm grown on silicon by organometallic vapor phase epitaxy. Compared with the same structure grown on a reference planar InP substrate, photoluminescence of the MQWs on Si shows both comparable line widths and internal quantum efficiencies at room temperature. A specially engineered InP buffer with interlayers on a nanopatterned silicon substrate was used. Cross-sectional transmission electron microscopy reveals effective dislocation filtering by the three strained InGaAs interlayers. The high-quality quantum-well structure grown on the InP-on-Si template suggests great potential of integrating III–V photonic devices on the Si platform.**

***Index Terms*— InAlGaAs/InAlAs multi-quantum wells, organometallic vapor phase epitaxy, photoluminescence, InP-on-Si.**

I. Introduction

QUARTERNARY alloys such as GaAlInAs and InGaAsP lattice-matched to InP have been widely used in photonic devices for semiconductor lasers [1], [2] emitting at 1550 nm or 1310 nm. Currently, InP has been the most prevailing substrate for homo-or pseudomorphic epitaxy of photonic devices as 'zero' defect is the convention wisdom for high performance. Even InP substrates can be produced in larger diameters, its inherent fragility requires a greater thickness that would further increase the already high substrate cost. Si substrate is a natural alternative and silicon photonics has been explored for over a decade, aiming for the eventual convergence of electronics and photonics. Photonic integrated circuits (PICs) on Si, which integrate planar photonic devices with the mature silicon manufacturing technology, have attracted great attention [3]. To this end, respectable results have been demonstrated by direct wafer bonding of active devices originally grown on InP substrates onto the silicon substrates. However, this technology is limited by the yield and complicated alignment [4]. On the other hand, hetero-epitaxial growth of InP on Si for photonics applications was attempted for a few decades but yet to result in high quality optical devices [5]. The main challenge lies in high defect density and stress from both lattice mismatch and thermal mismatch [6]. To effectively confine growth defects in the initial stage, nano-patterned growth was put forward, utilizing a two-step growth method [7] and aspect ratio trapping (ART) technique [8]. For the growth of InP-based planar optical and electrical devices, epitaxial lateral overgrowth (ELOG) [9] has been adopted and developed, not only for smooth thin film surface, but also for mitigating defect extension during coalescence. Moreover, strained interlayers and superlattices have been shown to provide great benefit to dislocation blocking and filtering [10].

Hetero-integration is of great importance for optoelectronic application, especially InP lasers on a Si platform. There have been very few reports on the direct growth of InP-based optical devices on silicon. The first InP-based laser integrated on Si has been demonstrated by Razeghi et al. [11]. In addition, Kataria et al. [12] reported InGaAsP/InP quantum-wells grown on ELOG of InP on Si. InAlGaAs-based quantum-well lasers, an alternative to the conventional InGaAsP-based systems, are drawing increasing attention nowadays due to the larger conduction-band offset [13]. This feature leads to better high temperature characteristics, improved efficiency and enhanced differential gain [14]. To the best of our knowledge, no investigation of InAlGaAs-based quantum wells epitaxially grown on Si substrates has been reported. In this letter, we report the growth and characterization of InAlGaAs/InAlAs MQWs deposited on an InP-on-Si (IoS) template. Low-temperature PL emission at $\sim$1.31 μm from the MQW was obtained.

II. Growth Procedure

The IoS template was grown on a nano-patterned Si substrate in an Aixtron AIX-200/4 horizontal OMVPE system. Preparation of the IoS templates has been reported in Ref. [15]. Initially, SiO_2 trenches and Si concaves, both 30 nm in width, were formed by top-down lithography and dry etching. After depositing low-temperature InP seed arrays inside the trenches, the SiO_2 dielectric was removed to avoid generation of new defects at the SiO_2/InP interface. A coalesced InP buffer layer was then overgrown on top of the seed arrays [15]. Within the 2.7 μm thick InP buffer layer, three 68 nm thick strained $In_{0.51}Ga_{0.49}As$ interlayers were inserted to serve as dislocation filters. The IoS template together with a reference semi-insulating planar InP (001) substrate was put in the OMVPE reactor side by side. A 200 nm InP buffer was first deposited, followed by the growth of five pairs of $In_{0.53}Al_{0.13}Ga_{0.34}As/In_{0.52}Al_{0.48}As$ quantum wells. All the epi-layers were unintentionally doped in this structure on the IoS template, as shown schematically in Fig. 1.

Manuscript received November 5, 2014; revised December 16, 2014; accepted January 6, 2015. Date of publication January 12, 2015; date of current version March 6, 2015. This work was supported by the Research Grants Council, Hong Kong, under Grant 614312 and Grant 614813.

The authors are with the Department of Electronic and Computer Engineering, Hong Kong University of Science and Technology, Hong Kong (e-mail: bshiaa@ust.hk; qli@connect.ust.hk; ywanab@ust.hk; eeepsd@gmail.com; eexinbo@ust.hk; eewilson@ust.hk; eekmlau@ust.hk).

Color versions of one or more of the figures in this letter are available online at http://ieeexplore.ieee.org.

Digital Object Identifier 10.1109/LPT.2015.2391099

1041-1135 © 2015 IEEE. Personal use is permitted, but republication/redistribution requires IEEE permission.
See http://www.ieee.org/publications_standards/publications/rights/index.html for more information.

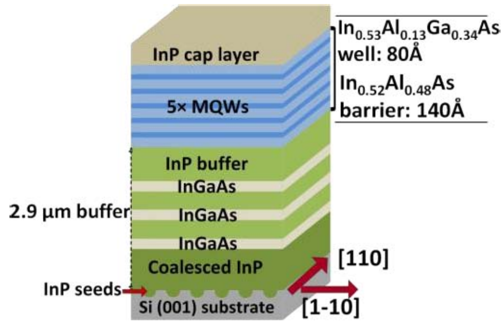

Fig. 1. Schematic of InAlGaAs/InAlAs MQWs on the InP-on-Si template with three strained InGaAs interlayers in the buffer.

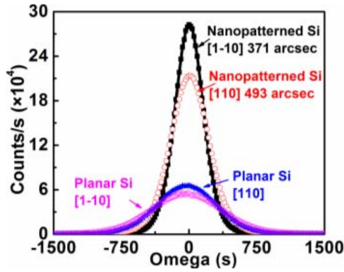

Fig. 2. XRD ω-rocking curves of the InP-on-Si template and the reference InP grown on planar Si substrate along the [110] and [1]–[10] directions, respectively.

The pressure in the OMVPE reactor during the InAlGaAs/InAlAs MQWs growth was maintained at 100 mbar. Triethylgallium (TEG), trimethylindium (TMI) and trimethylaluminum (TMA) were used as group III precursors, and tertiarybutylarsenic (TBA) was used as the group V precursor. Both the $In_{0.53}Al_{0.13}Ga_{0.34}As$ well and $In_{0.52}Al_{0.48}As$ barrier (lattice-matched to InP) were grown at 650 °C with a V/III mole ratio of 4.2 and 10.9, respectively. Finally, the MQW structure was capped with a 60 nm thick InP layer, for passivation and better carrier confinement for the PL measurement. High resolution x-ray diffraction (XRD) and atomic force microscope (AFM) were used to characterize the crystalline quality and surface morphology, respectively.

III. Characterization and Discussion

Fig. 2 shows the XRD ω-rocking curves of the as-grown IoS template without the MQW structures on top. With a total InP epi thickness of $\sim$2.7 μm on Si substrates, the full width at half maximum (FWHM) values of the (004) plane ω-scans along the [1]–[10] and [110] directions (defined as perpendicular and parallel to nano-trenches) are 371 and 493 arcsec, respectively. Based on Ayer's model [16], the upper bound defect density is calculated to be between 4.3 and 7.6 $\times$ 10^8 cm^{-2}. Compared with a 1.3 μm compositional graded InAlAs/GaAs buffer grown on offcut Si (FWHM of $\sim$1600 arcsec) [17], a four-fold reduction in FWHM and therefore one order lower defect density was achieved. The line width in the [1]–[10] direction is smaller because more effective defect interaction and confinement occurs in the direction perpendicular to the nano-patterned trenches [15]. For comparison, the results measured from a 2.3 μm thick buffer composed of 1.3 μm InP and 1 μm GaAs grown on a planar Si (001) substrate [16] was also presented. The FWHM values of the ω-rocking curves in [110] and [1–10] directions (defined as parallel and perpendicular to major flat) are 766 arcsec and 911 arcsec respectively, shown in Fig. 2.

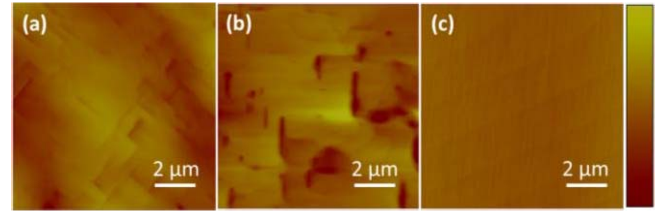

Fig. 3. AFM images of (a) 10 × 10 μm^2 area on the InP-on-Si substrate before QW growth with RMS = 3.63 nm; (b) 10 × 10 μm^2 area on the same InP-on-Si substrate after QW growth with RMS = 3.95 nm; (c) 10 × 10 μm^2 area on the QW grown on the InP reference substrate with RMS = 0.31 nm. Vertical color scale bar represents a depth range of 30 nm, 30 nm and 10 nm for (a), (b) and (c), respectively.

The anisotropic FWHM values on the planar Si are probably related to the observation that the low-temperature InP nuclei on GaAs buffer exhibited elongated structures instead of spherical-shaped dots. The significant line width reductions on the patterned Si clearly indicate an InP buffer with better crystalline quality, critical for the realization of efficient optoelectronic devices.

Surface morphology was investigated by AFM. As illustrated by the AFM images in Fig. 3, after the quantum-well growth, the root-mean-square (RMS) roughness of the IoS-based sample increased from 3.63 to 3.95 nm across a 10 × 10 μm^2 scanned area, indicating that the surface becomes slightly rougher. The rougher surface might be contributed by thickness variations in MQW regions. On the other hand, the identical MQWs on the InP substrate exhibited atomic step flow on the surface with a RMS value of only 0.31 nm across a 10 × 10 μm^2 area. The rougher surface observed in Fig. 3(b) can have negative impacts on the optical proficiency of the MQWs on the Si substrate, which is to be discussed in more details shortly.

In addition to the AFM characterization, we examined the defect distributions with cross-sectional TEM. Imaging was carried out using a JEOL2010F field-emission microscope operating at 200 keV. Taken along the [110] zone axis, the bright-field TEM image in Fig. 4(a) presents the whole structure. High density of defects, such as stacking faults (SFs) and threading dislocations (TDs), are generated at the hetero-interface between the Si substrate and the InP seed layer. Although most of the defects have been confined inside the concaves via epitaxial necking effect [15], a number of SFs and TDs still go beyond the concaves and propagate upwards. These SFs lie in {111} planes, as seen from the high-resolution TEM image in Fig. 4(b). These defects, however, bend and annihilate during the InP coalescence and overgrowth, leading to a reduced defect density beneath the first InGaAs interlayer. The three strained InGaAs interlayers further filter the upward propagating SFs and TDs, as demonstrated in Fig. 4(c). However, the filtering is not complete such that some defects, especially SFs, can penetrate through the InAlGaAs/InAlAs

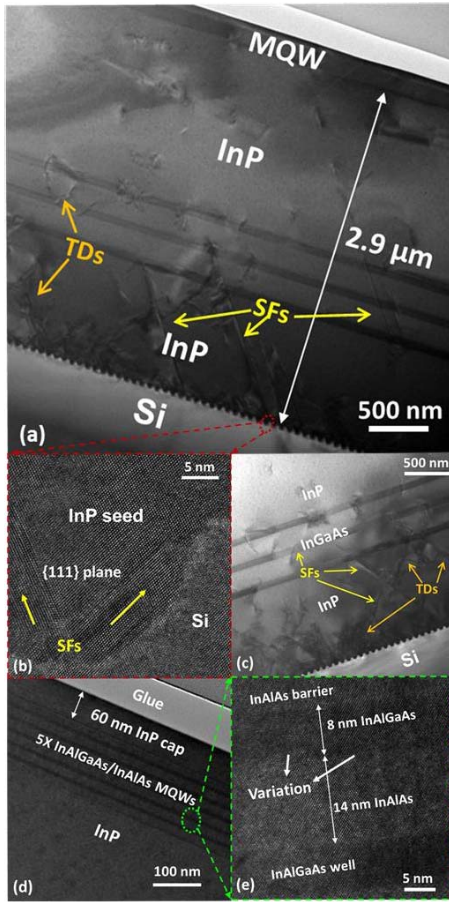

Fig. 4. [110] zone axis cross-sectional bright-field (a) low-resolution TEM image of the whole structure with a total buffer thickness of around 2.9 μm; (b) high-resolution TEM image of the interface between the Si substrate and the InP seed; (c) a portion of three InGaAs strained interlayers separated by InP, showing the dislocation filter function of these inserted layers; (d) TEM image of five periods of InAlGaAs/InAlAs MQWs grown at 650 °C. The dark regions indicate $In_{0.53}Al_{0.13}Ga_{0.34}As$ quantum-well parts and the bright regions imply $In_{0.52}Al_{0.48}As$ barriers; (e) high-resolution TEM image revealing thickness variations of the quantum well.

quantum wells, as observed in Fig. 4(a). Fig. 4(d) shows the TEM image of the MQWs grown on the IoS template. The SFs-dominated defects inevitably function as non-radiative centers and reduce the carrier recombination efficiency, which is of negative influence to optical device operation [18]. One drawback of using the trench pattern growth is the lack of capability to trap (111)-orientated stacking faults along the parallel direction of the trenches, which can be resolved by high aspect ratio nano-porous pattern, introduced by Ref. [19]. Besides, by adopting V-grooved Si substrates [20], defect generation can be further reduced because Si (111) is easier for III-V to nucleate compared to Si (001) and antiphase-domains can be avoided for III-V epitaxy on Si {111} planes.

The composition of In in the InAlGaAs wells was determined by XRD measurement, while Al composition was calculated based on room temperature PL [21], as depicted in Fig. 5(a). To compare the quality of InAlGaAs/InAlAs MQWs grown on the IoS template and on the reference planar InP (001) substrate, PL was conducted at both low temperature (15 K) and room temperature (RT), with excitation by a 300 mW all-solid-state 671 nm red laser.

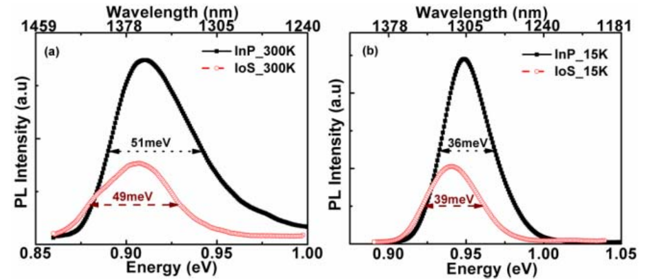

Fig. 5. Photoluminescence curves recorded at (a) room temperature (300 K) and (b) low temperature (15 K) for InAlGaAs/InAlAs MQWs grown on the InP-on-Si template and the InP reference substrate, respectively.

The PL spectra obtained at the two temperatures are displayed in Fig. 5(a) and (b). It is noted that, the peak emission intensities from the MQW on IoS are about 50% and 42% of the reference sample at RT and 15 K, respectively. However, the emission linewidths of the two samples are comparable, suggesting that the alloy composition is respectably uniform in the MQW on IoS. The slightly smaller FWHM in the IoS sample at RT is contributed by the stress from the underlying InP buffer grown on Si substrate. At RT, the central wavelength of PL is 1363 nm. When the temperature is lowered to 15 K, the peak wavelengths of both samples are blue shifted to ~1310 nm, shown in Fig. 5(b). To characterize the PL-efficiency, the integrated PL intensities of the IoS-based MQWs are calculated to be 43.2% and 47.1% of the InP reference at RT and 15 K, respectively.

The degraded PL peak intensity in the IoS-based MQWs can be attributed to three reasons: First, a rougher buffer surface [Fig. 3(b)] and thickness variations in the MQWs [Fig. 4(e)] led to more traps at the quantum well/barrier interfaces. These traps acted as non-radiative centers and lowered the emission intensity. XRD (004) ω-2theta scans show that the FWHM of the first-order MQW fringe for the IoS-based and InP-based samples are 150 arcsec and 91 arcsec, indicating a higher interface roughness of the IoS-based one. Second, as observed in the TEM images, although the ELOG of InP and the three strained InGaAs interlayers did block and eliminate most of the defects generated from the bottom interface between Si and the InP seed layer, the SFs-dominated defects that penetrated into upper MQWs would inevitably degrade crystalline quality of the MQWs, thus decreasing PL intensity in the IoS-based sample. Another important factor was related with the buffer beneath. The excited hot carriers generated in the InP buffer could have a quite long diffusion length (~1.4 μm) [22]. For the InP reference sample, these excited carriers diffused into MQWs and enhanced radiative recombination, as well as PL intensity. However, for the InP-on-Si substrate, due to smaller band gap of the three strained InGaAs interlayers (~0.76 eV), excited carriers generating from the InP buffer would be easily trapped by these InGaAs "wells" [23], preventing contribution of substrate to the PL intensity of MQWs. Besides, these "wells" could have a strong absorption of light scattering from the MQWs, which would also decrease the PL intensity.

To study the internal quantum efficiency (IQE) of the MQWs, temperature dependent PL of the IoS-based QWs

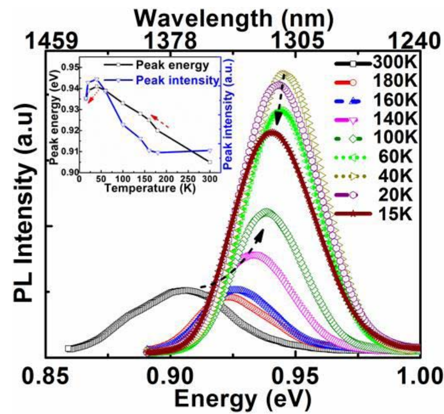

Fig. 6. Photoluminescence spectra recorded at various temperatures ranging from 300 K to 15 K (inset: peak PL energy and peak PL intensity variations according to different temperatures).

was measured, as shown in Fig. 6. From 300 K to around 40 K, the peak wavelength shifts from 1363 to 1311 nm with emission intensity increases by 3.22 times. However, as the temperature was further lowered from 40 K to 15 K, the trend was reversed. The intensity drops and the emission peak red shifts with decreasing temperature. This phenomenon was first observed in InAlGaAs material by Chua et al. [24], associated with multiple competing transitions and exciton localization, caused by disordered alloy atomic arrangement [25]. To further estimate the IQE variations of the QWs, we calculated the emission power by integrating over the PL spectra at different temperatures. Assuming the highest IQE at low temperature being 100%, the IQEs of the IoS-based and InP-based MQWs at RT are 37% and 45.4%, respectively. The comparable IQE at room temperature indicates a rather good IoS template quality and can be further improved through a better optimized multi-quantum wells design.

IV. Conclusion

In conclusion, lattice-matched InAlGaAs/InAlAs MQWs on an InP-on-Si substrate with three strained InGaAs interlayers have been grown by OMVPE and characterized. TEM revealed that the three interlayers can effectively filter most of the upward propagating defects. Furthermore, MQWs grown on the IoS template and on the reference InP substrate exhibited comparable line widths and internal quantum efficiencies at both RT and 15 K, although the intensity of the former is ~50% lower than the reference sample. The intensity reduction in the IoS-based MQW structure was attributed mainly to SFs-dominated defects propagation and interface roughness in the MQWs of the IoS-based structure. To further improve the PL intensities of the IoS-based MQWs, attention should be focused on achieving a smoother IoS substrate surface and lower defect density in the buffer.

References

[1] E. P. O'Reilly and M. Silver, "Temperature sensitivity and high temperature operation of long wavelength semiconductor lasers," *Appl. Phys. Lett.*, vol. 63, no. 24, pp. 3318–3320, 1993.

[2] J. Thompson, R. M. Ash, N. Maung, A. J. Moseley, and D. J. Robbins, "Long wavelength GRIN-SCH MQW lasers incorporating graded GaAlInAs confinement layers," *J. Electron. Mater.*, vol. 19, no. 4, pp. 349–355, 1990.

[3] L. A. Coldren, S. W. Corzine, and M. L. Mashanovitch, *Diode Lasers and Photonic Integrated Circuits*, vol. 218. Hoboken, NJ, USA: Wiley, 2012.

[4] G. Roelkens *et al.*, "III–V/Si photonics by die-to-wafer bonding," *Mater. Today*, vol. 10, nos. 7–8, pp. 36–43, 2007.

[5] M. Sugo, Y. Takanashi, M. Al-Jassim, and M. Yamaguchi, "Heteroepitaxial growth and characterization of InP on Si substrates," *J. Appl. Phys.*, vol. 68, no. 2, pp. 540–547, 1990.

[6] M. K. Lee, D. S. Wuu, and H. H. Tung, "Heteroepitaxial growth of InP directly on Si by low pressure metalorganic chemical vapor deposition," *Appl. Phys. Lett.*, vol. 50, no. 24, pp. 1725–1726, 1987.

[7] K. Ishida, "The two-step growth mechanism of MOCVD GaAs/Si," in *Proc. MRS*, 1987, pp. 133–138.

[8] T. A. Langdo, C. W. Leitz, M. T. Currie, E. A. Fitzgerald, A. Lochtefeld, and D. A. Antoniadis, "High quality Ge on Si by epitaxial necking," *Appl. Phys. Lett.*, vol. 76, no. 25, pp. 3700–3702, 2000.

[9] N. H. Julian, P. A. Mages, C. Zhang, and J. E. Bowers, "Improvements in epitaxial lateral overgrowth of InP by MOVPE," *J. Cryst. Growth*, vol. 402, pp. 234–242, Sep. 2014.

[10] M. Tang *et al.*, "1.3-μm InAs/GaAs quantum-dot lasers monolithically grown on Si substrates using InAlAs/GaAs dislocation filter layers," *Opt. Exp.*, vol. 22, no. 10, pp. 11528–11535, 2014.

[11] M. Razeghi *et al.*, "First cw operation of a $Ga_{0.25}In_{0.75}As_{0.5}P_{0.5}$-InP laser on a silicon substrate," *Appl. Phys. Lett.*, vol. 53, no. 24, pp. 2389–2390, 1988.

[12] H. Kataria *et al.*, "Simple epitaxial lateral overgrowth process as a strategy for photonic integration on silicon," *IEEE J. Sel. Quantum Electron.*, vol. 20, no. 4, Jul./Aug. 2014, Art. ID 8201407.

[13] J. Decobert, N. Lagay, C. Cuisin, B. Dagens, B. Thedrez, and F. Laruelle, "MOVPE growth of AlGaInAs–InP highly tensile-strained MQWs for 1.3 μm low-threshold lasers," *J. Cryst. Growth*, vol. 272, nos. 1–4, pp. 543–548, 2004.

[14] A. Tandon, D. P. Bour, Y. L. Chang, C. K. Lin, S. W. Corzine, and M. R. Tan, "Low-threshold, high-T_0 and high-efficiency 1300 nm and 1500 nm lasers with AlInGaAs active region grown by MOCVD," *Proc. SPIE*, vol. 5349, pp. 206–217, Jun. 2004.

[15] Q. Li, K. W. Ng, C. W. Tang, K. M. Lau, R. Hill, and A. Vert, "Defect reduction in epitaxial InP on nanostructured Si (001) substrates with position-controlled seed arrays," *J. Cryst. Growth*, vol. 405, pp. 81–86, Nov. 2014.

[16] Q. Li, X. Zhou, C. W. Tang, and K. M. Lau, "Material and device characteristics of metamorphic $In_{0.53}Ga_{0.47}As$ MOSHEMTs grown on GaAs and Si substrates by MOCVD," *IEEE Trans. Electron Devices*, vol. 60, no. 12, pp. 4112–4118, Dec. 2013.

[17] N. Mukherjee *et al.*, "MOVPE III–V material growth on silicon substrates and its comparison to MBE for future high performance and low power logic applications," in *Proc. IEEE Int. Electron Devices Meeting (IEDM)*, Dec. 2011, pp. 35.1.1–35.1.4.

[18] S. Mahajan, "Defects in semiconductors and their effects on devices," *Acta Mater.*, vol. 48, no. 1, pp. 137–149, 2000.

[19] K. Nishio, S. Tagawa, T. Yanagishita, and H. Masuda, "Fabrication of highly ordered nanoporous Si with high aspect ratio through prepatterning of Si using porous alumina mask," *Jpn. J. Appl. Phys.*, vol. 53, no. 7, p. 075201, 2014.

[20] W. Guo *et al.*, "Selective metal-organic chemical vapor deposition growth of high quality GaAs on Si (001)," *Appl. Phys. Lett.*, vol. 105, no. 6, pp. 062101-1–062101-3, 2014.

[21] D. Olego, T. Y. Chang, E. Silberg, E. A. Caridi, and A. Pinczuk, "Compositional dependence of band-gap energy and conduction-band effective mass of $In_{1-x-y}Ga_xAl_yAs$ lattice matched to InP," *Appl. Phys. Lett.*, vol. 41, no. 5, pp. 476–478, 1982.

[22] S. S. Li, "Determination of minority-carrier diffusion length in indium phosphide by surface photovoltage measurement," *Appl. Phys. Lett.*, vol. 29, no. 2, pp. 126–127, 1976.

[23] D. J. Westland, D. Mihailovic, J. F. Ryan, and M. D. Scott, "Optical time-of-flight measurement of carrier diffusion and trapping in an InGaAs/InP heterostructure," *Appl. Phys. Lett.*, vol. 51, no. 8, pp. 590–592, 1987.

[24] S. J. Chua and A. Ramam, "Photoluminescence observations in bandgap tailored InGaAlAs epilayers lattice matched to InP substrate," *J. Appl. Phys.*, vol. 80, no. 8, pp. 4604–4608, 1996.

[25] T. Yamamoto, M. Kasu, S. Noda, and A. Sasaki, "Photoluminescent properties and optical absorption of AlAs/GaAs disordered superlattices," *J. Appl. Phys.*, vol. 68, no. 10, pp. 5318–5323, 1990.